Geophysical Research Letters

Supporting Information For

Groundwater flow and exchange across the land surface explain carbon export patterns in continuous permafrost watersheds

B. T. Neilson[1*], M. B. Cardenas[2], M. T. O'Connor[2],

M. T. Rasmussen[1], T. V. King[1], and G. W. Kling[3]

[1]Civil and Environmental Engineering, Utah Water Research Laboratory, Utah State University, Logan, UT 84322, USA. [2]Department of Geological Sciences, Jackson School of Geosciences, The University of Texas at Austin, Austin, TX 78712, USA. [3]Department of Ecology and Evolutionary Biology, University of Michigan, Ann Arbor, MI 48109, USA.

*Correspondence to: bethany.neilson@usu.edu.

Contents of this file

Method S1

Field measurements. River discharge was monitored at the long-term main weir (Site 1, Figure S1) (serviced by University of Alaska at Fairbanks). Two trapezoidal flumes were installed seasonally farther upstream (Site 2 and Site 3). Both the weir and flumes were instrumented with pressure transducers that recorded water depth at 30- and 15- minute intervals, respectively, and were used to estimate volumetric discharge over time with stage-discharge rating curves developed from field measurements of stream flow. At the main weir, chemical samples were collected throughout the open water season, filtered through Whatman GF/F filters, acidified to pH $\sim$3, and stored cool and dark until analyzed for DOC and TDN on a Shimadzu TOC-V high-temperature Pt-catalyzed instrument with a nitrogen attachment [*Kling et al.*, 2000]. In the grid of shallow monitoring wells spanning the hillslope and riparian zone (Figure S1 and S4a), ground elevation, latitude, and longitude were determined using a Trimble S5 Robotic Total Station (Trimble Inc., Sunnyvale, CA) and control points were established using differential RTK GPS (Trimble R8, Dayton, OH). Using a marked metal rod and triplicate measurements, the depth of thaw below the ground surface and the corresponding elevation were also established for each well. Groundwater levels were measured from the top of the well casing. Groundwater chemical samples were collected from 37-62 locations on 5 Jul 2010, 19 Jul 2010, 12 Aug 2010, 28 Jun 2011, 14 Jul 2011, and 4 Aug 2011 at different locations in the riparian portion of the well grid (Figure S1c) using a 20-cm long steel needle to withdraw soil water that was filtered, stored, and analyzed as described above. Similar to the riparian wells, ground surface, thaw depth, and water surface elevations were established for the near-stream wells placed on river left and river right (Figure S1c). Each large stream pool (n=6) and well (n=12) was instrumented with an AquaTroll200 or LevelTroll400 (In Situ, Inc., Fort Collins, CO) pressure transducer that logged water level at 15 minute intervals to monitor the temporal variability of head gradients between the ground water and stream water.

Saturated hydraulic conductivity (*K)* was estimated in the field via in-situ slug tests as described by [*Surridge et al.*, 2005]. Slug tests were performed at depths ranging from 11 - 85 cm with a total of 26 measurements at 15 locations focused in the riparian area. A piezometer was driven in until refusal, which likely occurred at the top of the frozen soil, limiting the depth at which in-situ tests could be conducted. Water displacement during a slug test was measured with an AquaTroll700 pressure transducer placed at the bottom of the well. *K* was calculated by analyzing the water level recovery recorded by the pressure transducer following the theory of Bouwer and Rice [1976]. The slug tests lasted several seconds to a few minutes. Water level logging rates were typically set at 0.25 s. The *K* values from the slug test represents the effective horizontal *K* across the saturated length of the screen that varied depending on the height of the water table above the ice table, i.e., the saturated thickness of the aquifer. Laboratory measurements of *K* values from 0-20 cm in depth at 5 cm increments were also estimated from 7 sediment cores via a KSAT Benchtop Hydraulic Conductivity instrument (UMS Corp., Munich, DE).

Method S2

Vertically-explicit groundwater flow modeling. For the 'saturated' case, the water table (or water surface) coincides with the land surface, and therefore with the top boundary is a prescribed head boundary equal to the elevation. The other boundary conditions for this model were (Figure S3d):

(1) a no-slip bottom boundary condition at a given depth below the land surface that mimics surface topography due to the high correlation in surface and ice topography at small scales (Figure S2c, $R^2 = 0.87$), (2) a prescribed outflow velocity on the downstream vertical boundary (left side of Figure S3d), and (3) an open vertical boundary on the upstream side (right-side of Figure S3d).

For the inundated case, the steady Reynolds-averaged Navier-Stokes (RANS) equations were solved with the k-ω closure scheme [*Wilcox*, 1998] (Figure S3c, S5). The top boundary of the overland flow model represents the free water surface and is a slip/symmetry boundary with a uniform slope (Figure S3c). The downstream (left) boundary is prescribed an outflow velocity (and therefore flux) and the upstream boundary (right) is considered an open boundary which has no normal stress. Different outflow velocities were considered (0.01, 0.05, 0.1, 0.15, 0.2, 0.25 m s^{-1}). These velocities covered a broad range, but unfortunately we have no direct measurements from the field for comparison. However, anecdotally the velocities may be equivalent to a slow-flowing channel with magnitudes of a few centimeters per second. The bottom boundary (the land surface) is considered a no-slip wall. The RANS turbulent flow model calculates the pressure field and therefore it was sequentially coupled to an underlying groundwater flow model by imposing the calculated pressure at the bottom boundary of the inundated land surface (Figure S3c) as a prescribed pressure (Dirichlet) boundary at the top of the groundwater flow domain. The groundwater flow model solves the steady groundwater flow equation for a fully-saturated, heterogeneous, but locally isotropic, medium. The other boundaries of the groundwater flow model are: (1) a no flow right-side vertical boundary, (2) a prescribed uniform pressure left-side vertical boundary, and (3) a no flow bottom boundary representing the frozen soils.

Within both model cases, permeability and porosity decreased vertically with depth from the land surface. However, the permeability power function that represented this decrease with depth was slightly shifted upwards in order to avoid an unrealistically high permeability at the land surface. Porosity was found to decrease linearly with depth, was assumed to be uniform at depths greater than 20 cm, and was set to 1 at the land surface. This resulted in a step-wise linear porosity model (Figure S3b). Two average depths of the bottom boundary (or average thaw depths of 10 cm and 30 cm over the model domain) were also considered for each case of the vertically-explicit models. Additionally, although the turbulent surface flow model considered various flow rates or outflow velocity conditions, the depth of the inundating overland water was kept fixed at 20 cm at the outlet (left boundary).

The numerical flow and transport models were implemented with the generic finite-element model COMSOL Multiphysics. The turbulent overland flow model used a mapped mesh with quadrilateral elements. The minimum element size was 0.001 m and the maximum was 0.007 m. The node spacing increased gradually with a fraction of 1.1 from the bottom boundary (the wall) upwards. A boundary layer mesh was imposed on the bottom wall boundary by refining and subdividing the first quadrilateral element into 10 elements. The final mesh for the overland flow model had ~85,000 elements. The groundwater flow model used a free triangular mesh with minimum and maximum element sizes of 0.005 and 0.01 m, respectively, with the elements growing at a factor of 1.1 from the boundaries. This usually resulted in ~125,000 elements within the groundwater flow domain.

Method S3

Vertically-integrated groundwater flow modeling. In this application, the steady-state Boussinesq equation for saturated groundwater flow in an unconfined aquifer was linearized by assuming a known saturated thickness. This simple linearization is valid for broad and thin aquifers, such as the thawed layer in areas of continuous permafrost. This modeling approach arises from a vertical integration of the 3-D groundwater flow equation which leads to transmissivity, the product of the aquifer (or saturated zone) thickness and *K* [e.g., *Cardenas*, 2010]. With the collapse of the vertical dimension, the top (land surface) and bottom (frozen soil or ice table) boundaries become input parameters in the model because they define the saturated-zone thickness. For simplicity, we assume a spatially constant depth to the frozen soils. The vertically-integrated model is thus a planform 2-D model (flow is calculated in the *x*-*y* plane) where knowledge of the water table elevation, which follows the surface and subsurface frozen soil topography (Figure S2), allows for the calculation of the flow field (Figure S4) via the vertically-integrated form of the groundwater flow equation.

Topography was estimated from a 3-m resolution digital elevation model derived from fodar topographic maps for the basin (http://fairbanksfodar.com/fodar-earth). This single layer, vertically integrated model represents vertically averaged conditions within the saturated portion of the aquifer; therefore, we applied the average field-based *K* from all depths and locations plus or minus the standard deviation (0.66 m d^{-1} ± 0.47). These values were combined with an average porosity of 0.5 to estimate the range of expected groundwater contributions to the stream. The groundwater flow velocity and volumetric discharge was calculated at each node centered within each 3 m × 3 m cell based on the linearized Boussinesq equation. This amounts to a finite-difference calculation at each node. This calculation was implemented in ArcGIS, and so was the flow path visualization.

As stated above, for each vertically-integrated model analysis the groundwater flow estimates at the cells intersecting the stream were accumulated at Sites 1 and 2 in order to estimate volumetric groundwater flow rates ($Q_{gw,VI}$). These volumetric groundwater flow rates were then compared with in-stream volumetric discharge values from the weir or flume ($Q_{gw,W}$) (Table S2); the latter corresponds to the river discharge during baseflow conditions when the watershed had received no rain for some time and the hydrograph clearly represented baseflow recession.

Method S4

Direct estimates of groundwater fluxes into the stream. Near-stream groundwater flux calculations were estimated using field-based measurements of groundwater surface elevations from the near-stream wells, the in-stream water surface elevations, and the average field-based, saturated *K* ± 1 standard deviation (Eqn. 1) following Darcy's Law:

$$Q_{gw,D}(t) = -KA\frac{dh}{dx} \quad (1)$$

where *A* (m^2) is the area perpendicular to the groundwater flow that is calculated from the saturated aquifer thickness multiplied by one half of each stream pool circumference within the study reach (the wells were placed adjacent to the stream pools; see Figure S1c), *h* is the hydraulic

head between well and pool water surface elevation (m), and *x* is the distance between well location and pool edge of the water (m). Similar to above, the *K* in this analysis should represent that of the entire saturated thickness, and therefore is based on values from the slug tests which are inherently integrated across the saturated portion of the piezometer. The calculations provided groundwater inflow ($Q_{gw,D}$) directly to the stream from the layers below the very high *K* layers near the soil surface. The values were first normalized by the contributing watershed area to the 100-m long reach containing the stream pools with piezometers. The resultant discharge values per unit contributing area were extrapolated for the total contributing area at a given outlet, i.e., Site 1 or Site 2, and then compared to the groundwater contributions calculated from the VI model ($Q_{gw,VI}$) and measured directly by the weir ($Q_{gw,W}$) at the same outlet location (Table S2).

References:

Bouwer, H., and R. C. Rice (1976), A slug test for determining hydraulic conductivity of unconfined aquifers with completely or partially penetrating wells, Water Resources Research, 12(3), 423-428.

Cardenas, M. B. (2010), Lessons from and assessment of Boussinesq aquifer modeling of a large fluvial island in a dam-regulated river, Advances in Water Resources, 33(11), 1359-1366.

Kling, G. W., G. W. Kipphut, M. M. Miller, and W. J. O'Brien (2000), Integration of lakes and streams in a landscape perspective: the importance of material processing on spatial patterns and temporal coherence, Freshwater Biology, 43(3), 477-497.

Surridge, B. W. J., A. J. Baird, and A. L. Heathwaite (2005), Evaluating the quality of hydraulic conductivity estimates from piezometer slug tests in peat, Hydrological Processes, 19(6), 1227-1244.

Wilcox, D. C. (1998), Turbulence Modeling for CFD, 2nd ed., DCW Industries.

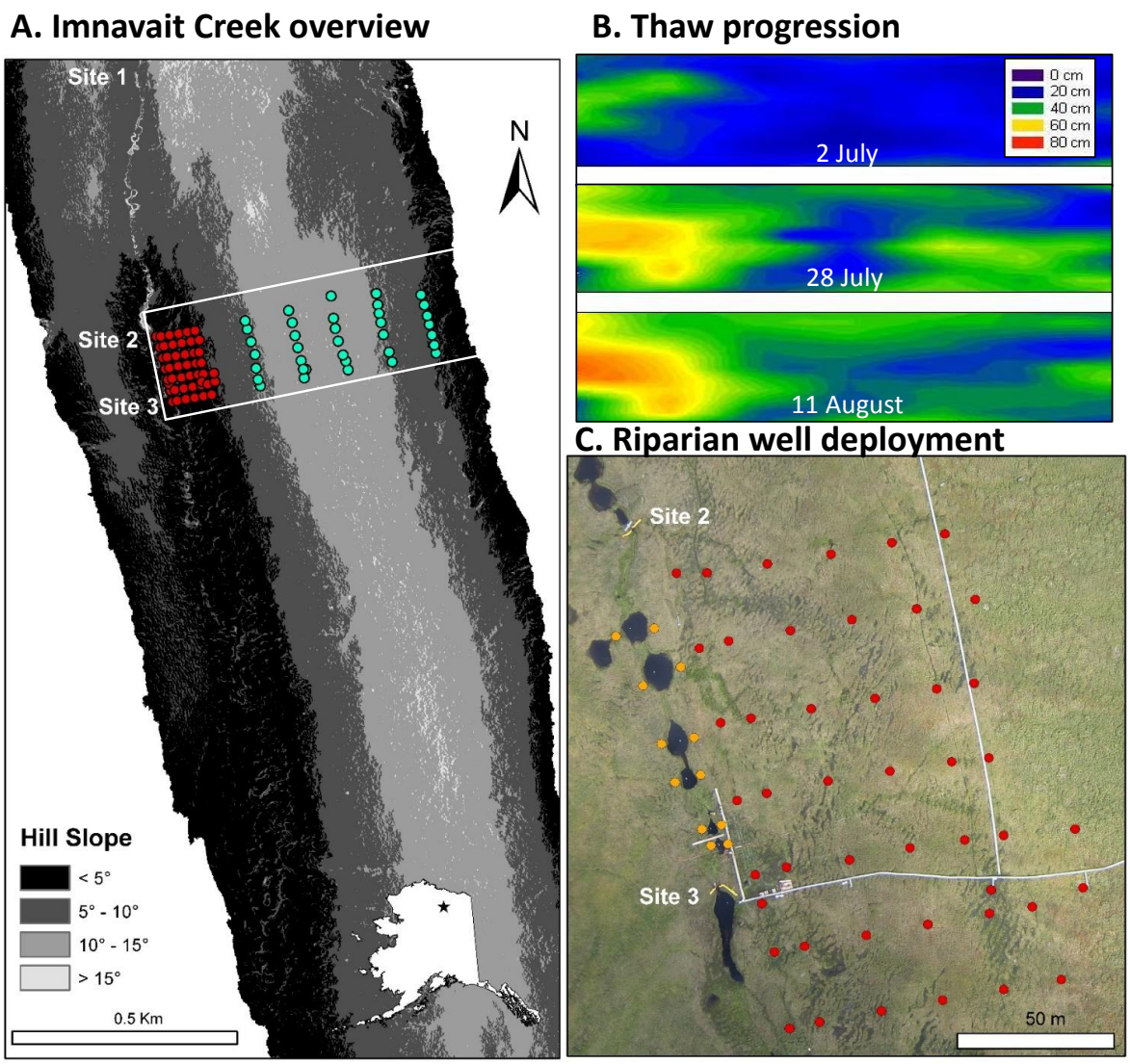

Figure S1. Imnavait Creek study area showing (A) the main weir (Site 1, draining 2.2 km^2), upstream flumes at Site 2, draining 1.42 km^2 and Site 3, draining 1.32 km^2, and well or piezometer locations in the riparian (red circles) and hillslope (blue circles) zones. (B) Depth to frozen soil or thaw progression in the hillslope and riparian zone throughout a summer season (hilltop on right, stream on left for the southern portion of the rectangle in (A). The Circumpolar Active Layer Monitoring (CALM) program (https://www2.gwu.edu/~calm/data/north.html) average end of season thaw depth data from the North Slope of Alaska between 1990-2016 shows range from 25.5 to 52 cm. (C) Riparian (red circle) and near-stream well (yellow circles) locations. The gray straight lines in the image are boardwalks used to access the sample locations.

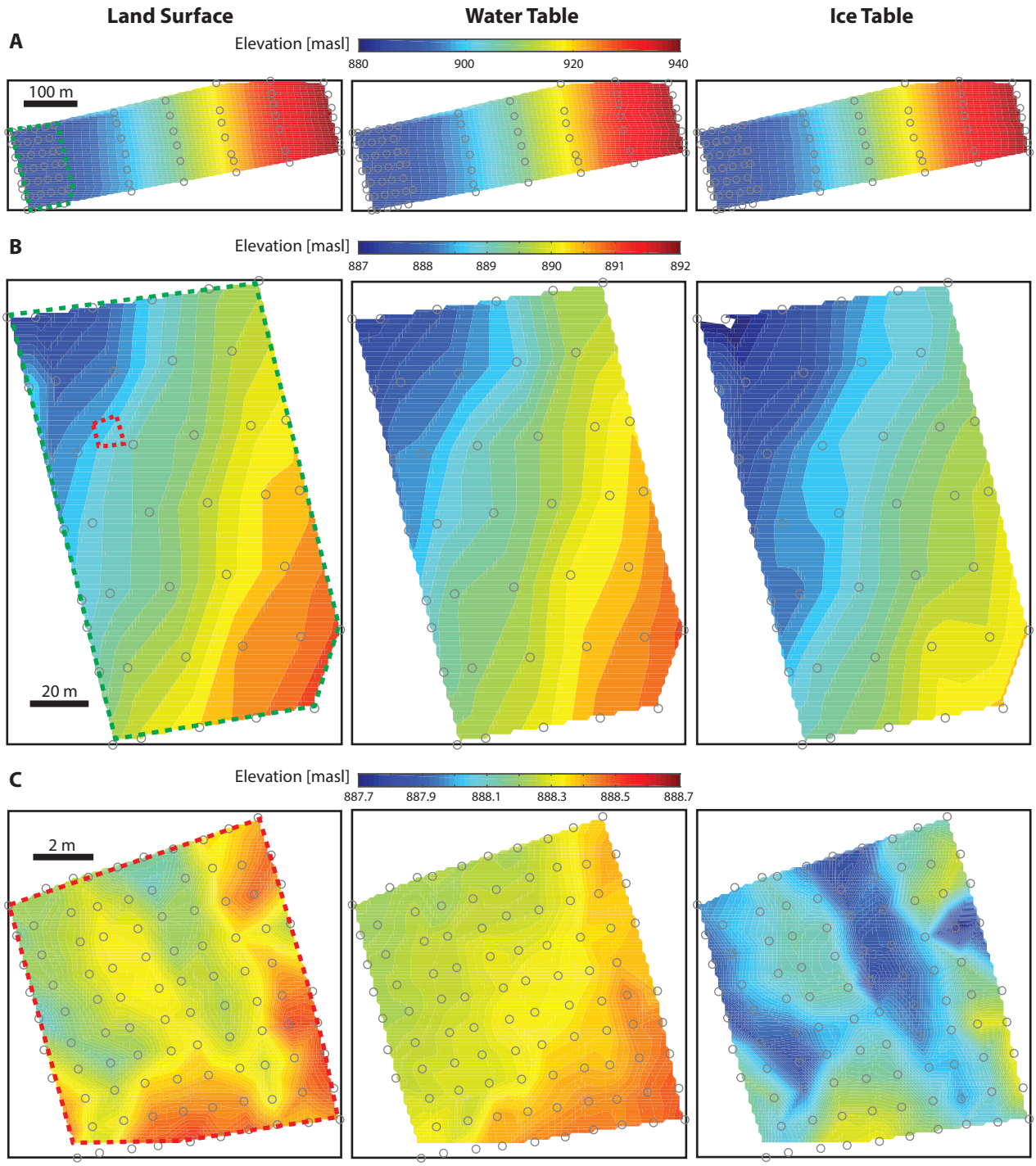

Figure S2. Observed land surface, water table, and frozen soil elevation for (A) a portion of the hillslope and riparian area (sampling grid in Fig. S1 and S4), (B) a more finely sampled portion of the riparian zone (green box in A), and (C) an even more finely sampled area within the riparian zone (red box in B). This telescoping sampling series illustrates that all three layers are strongly correlated at both macro- and micro-scales. Coefficients of determination between the individual measurement points of the land surface and the water table are 0.99 in (A), 0.95 in (B), and 0.80 in (C), and between the individual measurement points of the land surface and frozen soil are 0.99 in (A), 0.93 in (B), and 0.87 in (C).

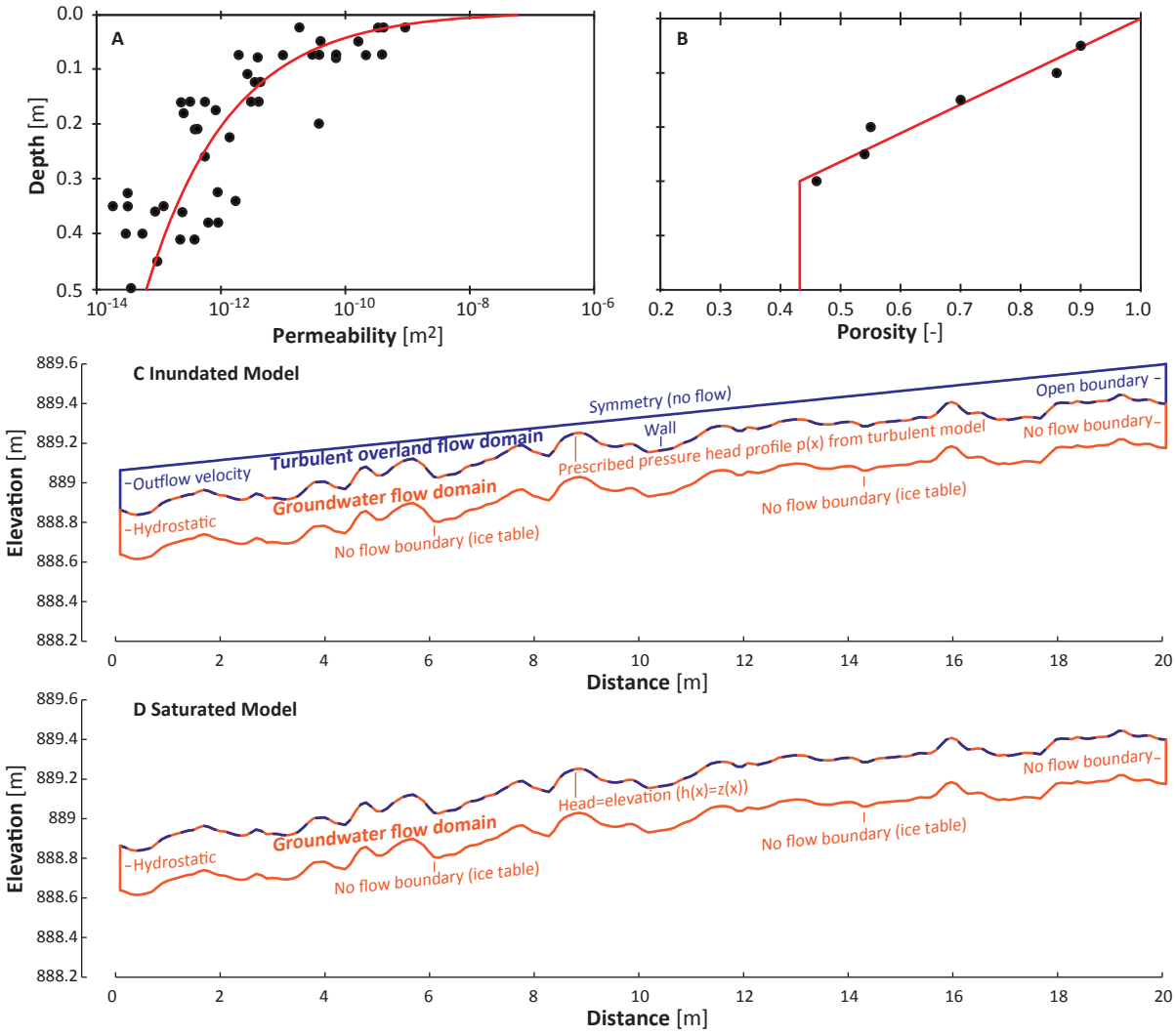

Figure S3. Diagram and data for the vertically-explicit modeling. (A) Permeability versus depth measurements (points) and model fit (line) that was applied within the vertically-explicit model. Hydraulic conductivity, K (m s^{-1}) = k * g/v, where k is the intrinsic permeability of the soil (m^2), g is gravity (m s^{-2}), and v is kinematic viscosity of the water (m^2 s^1). (B) Porosity (fraction) versus depth measurements (points) and model fit (line) that was applied within the vertically-explicit model. Model domain and boundary conditions for the (C) vertically-explicit inundated model where a turbulent overland flow model is sequentially coupled with a groundwater flow model (Figure 2a and S5), and (D) vertically-explicit saturated model (Figure 2c).

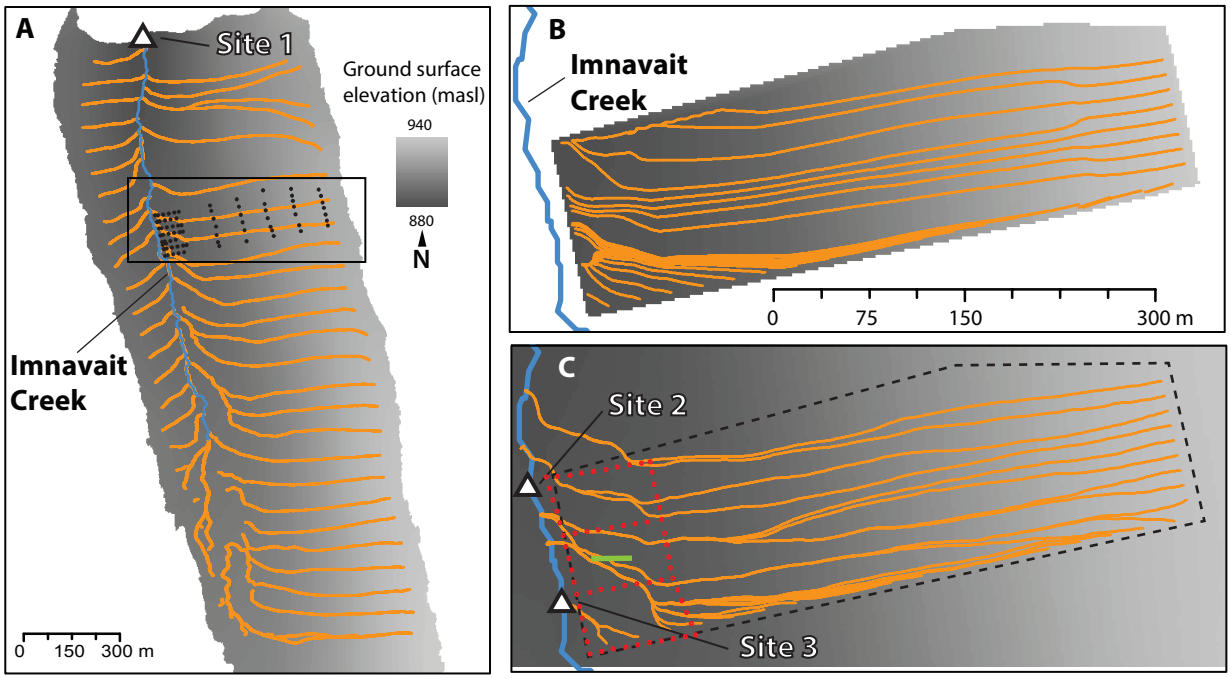

Figure S4. Map of sampling and monitoring locations and groundwater flow paths. (A) Observation points for co-located groundwater table and ice-table elevation measurements (black dots), weir location of discharge and chemical sampling (white triangles), and modeled groundwater flow paths from arbitrary start points near the hillslope crest (orange lines). (B) Groundwater flow paths based on measured water-table elevations. (C) Groundwater flow paths based on a vertically-integrated groundwater flow model and sampling locations for groundwater DOC (red circles, also shown in part in Figure S1c). The green line represents the transect used for the vertically-explicit modeling. The rectangle in (A) corresponds to the boundaries of (B) and (C), and the dashed line in (C) corresponds to the gray-filled area in (B).

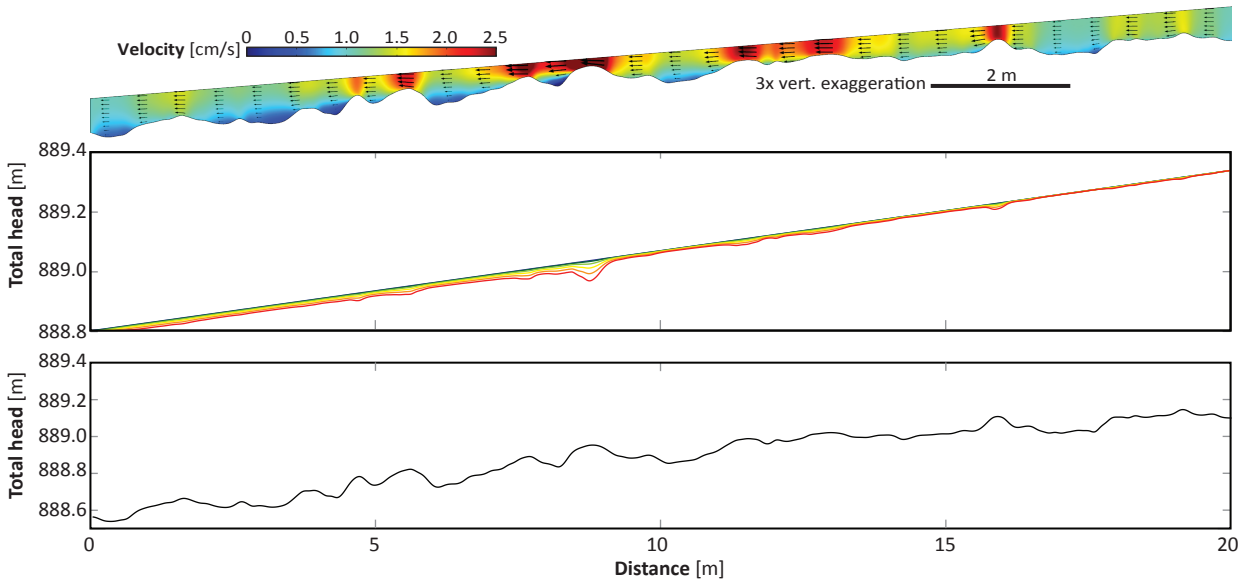

Figure S5. Vertically-explicit modeling results of a 20 m downslope transect within the riparian zone under inundated conditions (Figure S3c). Top: Turbulent overland flow velocity (cm s-1) field with a 3x vertical exaggeration. Middle: Total head profiles (colored lines) along the land surface, including the pressure head contributions (dynamic and hydrostatic) and the elevation head, from the turbulent flow model used as the boundary condition for the top of the groundwater model. Bottom: Land surface.

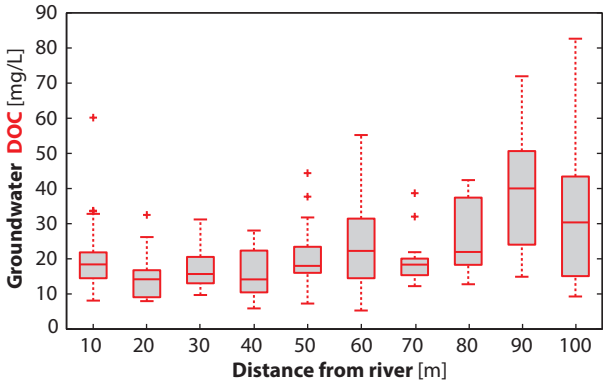

Figure S6. Dissolved organic carbon (DOC) concentrations (mg L^{-1}) for groundwater sampled in 2010-2011 at 10-20 cm depth in 10 m increments (see red dots in S4c) away from the stream at Imnavait Creek (boxplots show the mean and quartiles with outliers labeled by crosses). The samples from 10-40 m away from the stream were used for calculating the groundwater range in Figure 3.

Table S1. Comparison of integrated fluxes from the vertically-explicit models of inundated (0.2 m overland flow depth at the downstream left outlet), ponded, and saturated but not inundated conditions for a ~20 m long portion of the riparian zone. Overland flow fluxes were calculated by integrating the velocity along the entire depth of overland flow at the domain outlet (left boundary). Groundwater efflux is the integral of outward flux along the entire top boundary of the groundwater flow model domain (the land surface). The flux ratio is the ratio of these two fluxes, surface and groundwater efflux, and provides information on the amount exchanged across the land surface to that leaving the domain via overland flow. It is a metric for the amount of groundwater that exchanges with overland flow. Similar results for the (A) shallow (0.10 m) and (B) deeper thaw depth (0.30 m) illustrate that surface velocities and shallow soils are controlling exchanges, and deeper thaw does not translate into substantially greater exchanges or vertical mixing.

Model scenario	*Mean surface velocity ($m\ s^{-1}$)*	*Overland flow flux ($m^2\ s^{-1}$)*	*Groundwater efflux ($m^2\ s^{-1}$)*	*Flux ratio for 20-m of hillslope*	*Flux ratio per m*	*Turnover length (m)*
A. Thaw depth of 0.1 m at left boundary of groundwater model domain						
Inundated	0.010	2.0×10^{-3}	1.36×10^{-3}	0.678	0.034	29.5
Inundated	0.050	1.0×10^{-2}	1.36×10^{-3}	0.136	0.007	146.6
Inundated	0.100	2.0×10^{-2}	1.40×10^{-3}	0.070	0.003	286.5
Inundated	0.150	3.0×10^{-2}	1.46×10^{-3}	0.049	0.002	410.7
Inundated	0.200	4.0×10^{-2}	1.57×10^{-3}	0.039	0.002	507.8
Inundated	0.250	5.0×10^{-2}	1.76×10^{-3}	0.035	0.002	569.5
Ponded	N.A.	N.A.	9.98×10^{-4}	N.A.	N.A.	N.A.
Saturated	N.A.	N.A.	2.80×10^{-3}	N.A.	N.A.	N.A.
B. Thaw depth of 0.3 m at left boundary of groundwater model domain						
Inundated	0.010	2.0×10^{-3}	1.35×10^{-3}	0.677	0.034	29.6
Inundated	0.050	1.0×10^{-2}	1.36×10^{-3}	0.136	0.007	146.9
Inundated	0.100	2.0×10^{-2}	1.39×10^{-3}	0.070	0.003	286.9
Inundated	0.150	3.0×10^{-2}	1.46×10^{-3}	0.049	0.002	411.2
Inundated	0.200	4.0×10^{-2}	1.57×10^{-3}	0.039	0.002	508.5
Inundated	0.250	5.0×10^{-2}	1.75×10^{-3}	0.035	0.002	570.1
Ponded	N.A.	N.A.	1.07×10^{-3}	N.A.	N.A.	N.A.
Saturated	N.A.	N.A.	2.80×10^{-3}	N.A.	N.A.	N.A.

Table S2. Groundwater contributions based on the cumulative values estimated from the vertically-integrated modeling ($Q_{gw,VI}$ (L s^{-1})) at Site 1 and Site 2 shown in Figure S1 using the average in-situ hydraulic conductivity, *K*. $Q_{gw,W}$ (L s^{-1}) represents the measured baseflow condition at each location from 8-11 July 2014. $Q_{gw,D}$ (L s^{-1}) is the predicted gain of groundwater over the 100-m reach moving downstream from Site 3 to Site 2 (Figure S1) based on the local Darcy flux estimates extrapolated for the entire contributing drainage area. Values in parentheses for the weir measurements ($Q_{gw,W}$) show the standard deviation of these observations, and values in parentheses for the corresponding model results ($Q_{gw,VI}$) show the modeled range from applying the mean *K* plus or minus the standard deviation.

	Area (km^2)	**$Q_{gw,VI}$ (L s^{-1})**	**$Q_{gw,W}$ (L s^{-1})**	**$Q_{gw,D}$ (L s^{-1})**
Site 1	2.2	0.81 (0.23-1.39)	2.7 (0.8)	
Site 2	1.42	0.27 (0.08-0.46)	3.7 (1.2)	0.40 (0.11-0.67)

Table S3. DOC groundwater concentrations from depth profiles at two locations within the Imnavait Creek basin. Spec Cond is the specific electrical conductivity of the water (at 25 °C).

Date	**Depth** (m)	**Temp** (°C)	**Spec Cond** (µS cm^{-1})	**DOC** (mg L^{-1})
Site A, 30 Jul 2007	0.10	11.70	21.7	12.1
Site A, 30 Jul 2007	0.30	10.01	24.5	15.9
Site A, 30 Jul 2007	0.45	9.90	44.0	20.5
Site B, 30 Jul 2007	0.10	8.90	13.3	9.6
Site B, 30 Jul 2007	0.15	8.70	17.8	11.4
Site B, 30 Jul 2007	0.30	7.50	23.9	13.9